Simple random matrix model for the vibrational spectrum of structural glasses

E. Stanifer, P. K. Morse, A. A. Middleton, and M. L. Manning

Phys. Rev. E **98**, 042908 — Published 25 October 2018

DOI: 10.1103/PhysRevE.98.042908

A simple random matrix model for the vibrational spectrum of structural glasses

E. Stanifer, P.K. Morse, A.A. Middleton, M.L. Manning
Syracuse University Department of Physics

To better understand the surprising low-frequency vibrational modes in structural glasses, where the density of states $D(\omega)$ deviates from mean field predictions, we study the spectra of a large ensemble of sparse random matrices where disorder is controlled by the distribution of bond weights and network coordination. We find $D(\omega)$ has three regimes: a very-low frequency regime that can be predicted analytically using extremal statistics, an intermediate regime with quasi-localized modes, and a plateau in $D(\omega)$. When there is a finite probability of bond weights approaching zero strength, the intermediate regime displays a scaling consistent with $D(\omega) \sim \omega^4$, independent of network coordination and system size, just as in simulated structural glasses.

The vibrational spectra of disordered glassy materials exhibit universal features. Although these features govern the mechanical response and provide insight into mechanisms for material failure, their origin remains poorly understood.

Perhaps the most well-studied feature of the density of vibrational states $D(\omega)$ is the boson peak, which is an excess of vibrational modes above the Debye prediction, $D(\omega) \propto \omega^{d-1}$ [1–3]. In jammed packings the frequency at which the peak occurs, ω^*, scales linearly with the average excess number of contacts δz above the isostatic point where the number of constraints equals the degrees of freedom [2, 4, 5]. Additionally, the eigenvector statistics of modes in the boson peak follow a universal distribution [6].

Recently, another universal feature has been identified in simulations of low-dimensional jammed systems: $D(\omega) \sim \omega^4$ below ω^* [7–9], which deviates from recent mean-field calculations for the spectra in infinite dimensions that predict $D(\omega) \sim \omega^2$ [10, 11]. This interesting behavior has also been found in Heisenberg spin glass systems [12]. Understanding this regime is important, as the vibrational modes are quasilocalized and help govern flow and failure in disordered solids [1, 12–17].

Given the success of random matrix theory in predicting universal features in other physical systems [18, 19],it is natural to wonder if a random matrix model may also explain the ω^4 scaling in jammed packings. Other features, including the boson peak, have already been understood in terms of Euclidean random matrices, which are dynamical matrices for a set of points that are randomly and uniformly distributed in space [20].

Although there are generic arguments that the global minima of random functions should have a spectrum that scales as ω^4 [21], we would like to construct a random matrix model to provide insight into how features of the ω^4 region, such as the prefactor, or the location of the scaling regime, change with parameters such as the excess coordination δz. Such an understanding is important for predicting how material preparation protocols alter the mechanical response of glassy materials.

We study matrices that share three important features with the dynamical matrix: they are symmetric, positive semidefinite, and force balancing. In higher dimensions, force balance corresponds to d sum rules on partial sums of entries in each row of a matrix, while in 1D, the force balancing restriction simply requires the sum over all the entries in a row must be zero [1]. This rule is also obeyed by standard or weighted Laplacians, L_{ij}, which are also symmetric and positive semi-definite. They are defined by

$$L_{ij} = \begin{cases} -k_{ij} & i \text{ and } j \text{ are connected,} \\ \sum_{l \neq i} k_{il} & i = j, \\ 0 & \text{Otherwise,} \end{cases} \tag{1}$$

where k_{ij} is the independently chosen random weight of the edge between particles i and j and in the special case of the standard Laplacian, $k_{ij} = 1$ [22]. Standard Laplacian matrices are well-studied and possess distinctive vibrational spectra [23–26], so we focus on weighted Laplacians for the remainder of this article.

In order to calculate the Laplacian we must specify the topology of the underlying graph. Although recent advances have been made in analytically characterizing the spectra of Laplacians on an Erdős-Rényi graph [27, 28], Erdős-Rényi networks are not locally isostatic, as a significant fraction of nodes are under-coordinated (fewer than isostatic coordination $z_c = 2d$), which leads to highly localized excitations that are not seen in jammed packings [27].

Instead, we consider the weighted Laplacian on a z_c-regular graph with a small number of additional edges, or crossbonds. Since weighted Laplacians only obey one sum rule, they are effectively 1D and $z_c = 2$. The number of additional bonds is $\delta z N$ where N is the number of points and δz is the excess coordination.

Another important control parameter is the distribution of the edge weights and, in particular, the weight of this distribution near zero. We choose to parameterize this distribution as a power law with exponent α, normalized so that the mean is 1, $\rho(k) \propto k^\alpha$ on $\left[0, \frac{\alpha+2}{\alpha+1}\right]$. A uniform distribution corresponds to $\alpha = 0$ and we only consider normalizable distributions, $\alpha > -1$.

Finite size scaling for the weighted ring: We first study the finite size scaling of the low frequency excitations at isostaticity, when $\delta z = 0$ and the underlying network topology is simply a ring of size N. Although this

is a well-studied model, we believe its finite-size scaling can provide insight into the case with $\delta z > 0$.

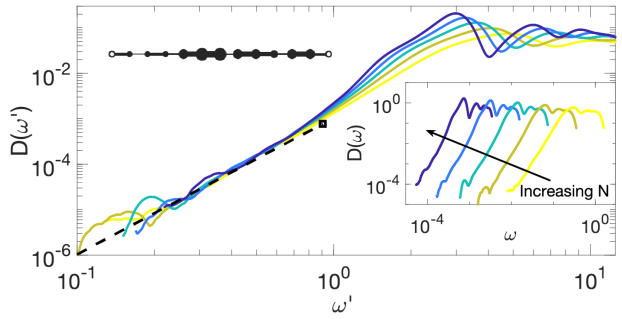

Figure 1: The rescaled density of states, $D(\omega')$ where $\omega' = \omega N$, for the two-regular graph with N=16, 64, 256, 1024, and 4096 and $\alpha = 0$, normalized by system size, N, averaged over at least 10^6 matrices. The analytic prediction for the low-frequency scaling is shown as the black dashed line. In the upper-left we have a sketch of a 1d chain with periodic boundary conditions (the open circles are the same node) **Inset:** Unscaled density of states, $D(\omega)$.

The inset to Fig. 1 shows the sample averaged density of states for $\alpha = 0$, calculated via diagonalization of the matrix, as a function of system size N, averaged over 2×10^6 matrices. The main panel shows the sample averaged density of states as a function of the normalized frequency, $\omega' = \omega N$, highlighting a region of power-law scaling at the lowest frequencies that disappears in the thermodynamic limit.

We hypothesize that the lowest-energy mode on a weighted ring is well approximated by a stretching of the two weakest bonds, with all other bond lengths relatively fixed. We expect this to be the case when $\alpha \leq 0$, so that the weight of the lowest two bonds are well separated from bonds with larger values of k_{ij}, especially in the limit of low ω, $\omega < N^{-\frac{2\alpha+3}{4\alpha+3}}$.

If the two weakest bonds have strengths k_1 and k_2 and are separated by m nodes, the frequency of this mode is $\sqrt{\frac{N(k_1+k_2)}{m(N-m)}}$. As we show in the supplement, one can use extremal statistics to find the exact distribution of the weakest bonds on the ring to predict that the low-frequency density of states scales as:

$$D(\omega) \propto N^{2\alpha+3}\omega^{4\alpha+3} \tag{2}$$

For a uniform distribution of bond weights ($\alpha = 0$), the contribution of these modes to the density of states scales as $(N\omega)^3$. The scaling of Eq. 2, using $\alpha = 0$, is shown as the black dashed line in Fig. 1.

Crossbonded ring with uniform bond weights: We hypothesize that adding a small number of crossbonds alters the low-frequency behavior by reducing the effective distance between the two weakest bonds. In the case of $\delta z = 0$, the two weakest bonds separate the ring into two segments that can move relative to one another at nearly zero cost, but if a crossbond connects those two segments it will significantly increase the energy of that mode. Therefore, the weak bonds that contribute to low-frequency modes must both be in a segment between crossbonds. Because there are $N\delta z$ such segments, we expect that crossbonds give rise to an extensive number of low-energy modes, so that the scaling regime described in the previous section persists in the thermodynamic limit.

We search for very low-weight edges that generate a two-cut of the network: two edges that, if removed, disconnect the network. In the supplement, we show the low-frequency density of states scales as

$$D_\alpha(\omega) \propto \left(\frac{1}{\delta z}\right)^{2\alpha+3} \omega^{4\alpha+3}, \tag{3}$$

independent of system size. In this equation, the term $\frac{1}{\delta z}$ takes the place of the term proportional to system size in the weighted ring (Eq. 2). The excess coordination effectively rescales the system, promoting a finite size effect seen in the vibrational spectrum of the ring to a thermodynamic property of the crossbonded system.

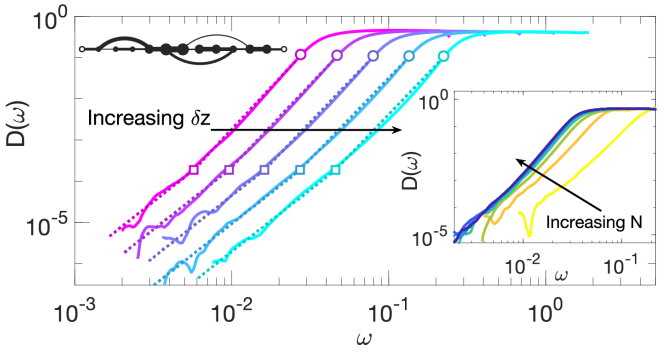

Figure 2: The density of states for fixed system size (N=1000) and changing $\delta z = 0.1, 0.168, 0.282, 0.476, 0.8$ In the upper-left we have a sketch of a 1d chain with periodic boundary conditions (the open circles are the same node) with additional bonds. **Inset:** The density of states, $D(\omega)$, for fixed $\delta z = 0.1$ and changing system size $N = 20$, 60, 120, 240, 500, 1000, 2000, and 4000.

To test the universal form predicted by Eq. 3, we computed the spectrum $D(\omega)$ for rings with crossbonds and uniform bond weights ($\alpha = 0$). For each value of δz and N we generated between 10^5 and 2×10^6 matrices [29], with independently chosen weights and uniformly random placements of the endpoints of the $N\delta z/2$ crossbonds. The inset to Fig. 2 displays plots of the sample-averaged density of states $D(\omega)$ for fixed $\delta z = 0.1$ as N increases. This example plot supports the convergence of $D(\omega)$ to a gapless distribution as $N \to \infty$. The main panel of Fig. 2 displays the computed density of states (solid lines) for large N ($N = 1000$) and varying δz. The dashed lines in Fig. 2 show fits of the form $D(\omega) \propto \omega^3$ to the low frequency region, as predicted by Eq. 3. These fits are in good agreement with the computed spectra.

Based on Eq. 3 and the more complete form of the density of states derived in Appendix B, we expect a collapse of $D(\omega)$ when frequencies are scaled by δz, for $\alpha = 0$. Fig. 3(a) shows the density of states for the scaled frequency, $\omega = \omega/\delta z$. For $\delta z = 0.168$ we numerically identify a frequency ω_e that best separates the ω^3 scaling regime from the remaining spectrum. Eq. 3 then predicts

that all other cutoff frequencies should scale linearly with δz, which is in good agreement with the data as shown by the open squares in Fig 2 and 3(a).

In addition to the crossover at ω_e, there is a second crossover where $D(\omega)$ flattens to a plateau. In jammed packings at zero temperature, where the boson peak occurs at the onset of the plateau, ω^* is often defined as the frequency at which the density of states attains a fixed fraction f (typically 25 %) of its value in the plateau [30]. We use that same definition here with $f = 0.25$.

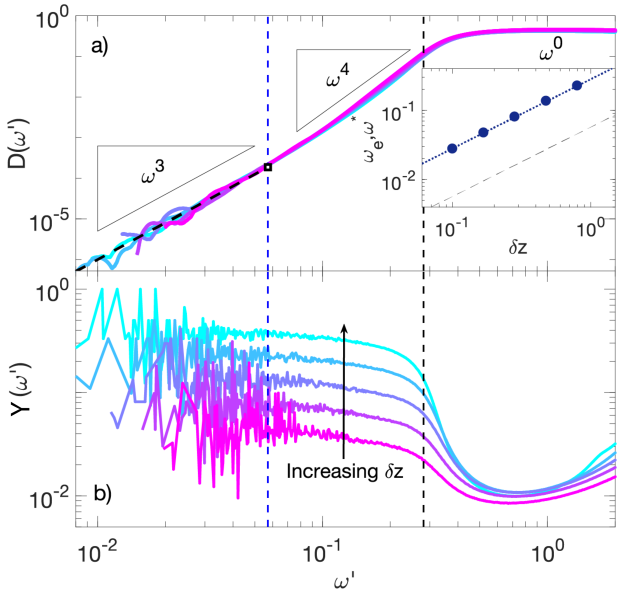

Figure 3: **a)**The density of states, $D(\omega)$, rescaled by δz, $\omega' = \omega/\delta z$. The blue dashed line indicates the transition from the ω^3 regime to the ω^4 regime while the black dashed line indicates the transition to the plateau. The inset shows the scaling of ω^* and ω_e with δz is linear. **b)**The inverse participation ratio, IPR, rescaled by δz. The IPR approaches a quasilocalized plateau in the ω^3 region.

In many disordered solids, numerical evidence suggests $\omega^* \propto \delta z$ [2, 5]. To check whether this is also true for our matrices, we plot the density of states as a function of the rescaled frequency $\omega' = \omega/\delta z$, for various values of δz, shown in Fig 3(a). We see a good collapse of the three regions, suggesting that both crossovers are linear in δz, which is also highlighted by the inset to Fig 3(a).

Importantly, this confirms that although the intermediate region between the two crossover frequencies spans less than a decade in frequency, it is well-defined and does not change as a function of excess coordination or system size. Specifically, these results mandate the following functional form for the density of states in our random matrix model with $\alpha = 0$:

$$D(\omega) = \begin{cases} \left(\frac{\omega}{\delta z}\right)^3 & \omega \leq \omega_e \\ \propto \omega^{\psi} & \omega_e \leq \omega \leq \omega^* \\ \propto const & \omega^* \leq \omega \end{cases} \quad (4)$$

To extract the scaling of $D(\omega)$ below the boson peak, we fit $D(\omega)$ to this functional form and extract the best-fit ψ for each value of δz (See table in supplemental materials). We find that all curves are consistent with $\psi = 4.0 \pm 0.05$ for frequencies $\omega_e \leq \omega \leq \omega^*$. This suggests $D(\omega) \propto \omega^4$, just as seen below the plateau in simulations of jammed packings.

Given the striking similarities between the density of states in this simple model and jammed packings, we would also like to know if the eigenvector statistics are similar. In jammed systems, many modes at frequencies below the boson peak are quasilocalized [30]. This is quantified by the inverse participation ratio (IPR), $Y(\omega) = \sum_i v_i^4 / (\sum_i v_i^2)^2$, where v is the vector associated with the eigenfrequency ω. In Fig 3(b), the very low-frequency regime of the IPR plateaus, and the value of this plateau scales with δz, indicating that only about $\frac{1}{\delta z}$ nodes are participating in the vibration. We have also shown in the supplemental materials that the value of the IPR is independent of system size in this quasi-localized regime.

Interestingly, the intermediate region exhibits values of IPR that are typically associated with quasilocalized excitations. Moreover, the size of those excitations seems to decrease as δz increases. In jammed solids, an outstanding open question is how the size of localized excitations changes as one approaches the jamming transition.

Crossbonded ring with power-law bond weights: Having a simple constructive model that reproduces many features of the vibrational modes in jammed packings is useful, because we can vary the model and ask what features are necessary to generate the ω^4 scaling in the density of states. One natural choice is to perturb the distribution of bond strengths away from the uniform distribution by changing the power-law exponent α.

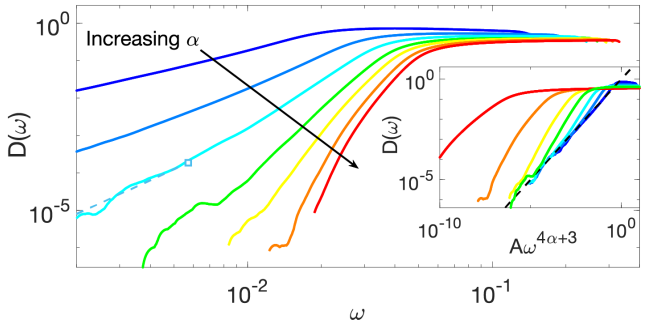

Figure 4: The density of states for $\alpha = -0.4, -0.2, 0, 0.25, 0.5, 1,$ and 2, with $\delta z = 0.1$. **Inset:** $D(\omega' = A\omega^{4\alpha+3})$ for the same values of α as in the main figure, where A is the coefficient predicted in Appendix B. The black dashed line is the predicted scaling for the low frequency regime.

For $\alpha > 0$, very weak bonds become rare and the assumptions that lead to Eq. 3 break down. Numerically, we observe that a gap appears to open up in the spectrum as α increases, as seen in Fig 4. For $\alpha < 0$, we expect Eq. 3 should still hold, as shown by the numerical data in the inset of Fig 4. In this case, however, the crossover frequency no longer scales linearly with δz, and so the power-law scaling between ω_e and ω^* – the exponent ψ

in Eq. 4 – is no longer independent of δz. In other words, an intermediate regime consistent with $D(\omega) \propto \omega^4$, independent of δz, is only possible for $\alpha = 0$. It seems that having finite probability of bonds with weight approaching zero provides for approximate ω^4 scaling.

Discussion: In this article, we propose a simple random matrix model that is locally nearly isostatic and captures features of the vibrational states of disordered packings that are typically associated with marginality. Specifically, the model recapitulates a plateau in the density of states above ω^*, and a regime consistent with ω^4 scaling immediately below that. Our model also has a second crossover frequency ω_e, below which $D(\omega)$ scales as ω^3.

The modes in this extremely low frequency regime are governed by extremal statistics, and so we can calculate their properties analytically. This allows us to demonstrate that ω_e scales linearly with excess coordination δz if and only if the weak bonds are uniformly distributed, suggesting that ω^4 seen in jammed packings arises due to a special, self-organized distribution of the weakest bonds.

Of course, jammed packings only exist in dimensions greater than unity. Above one dimension, the bond between particles is described by a tensor and not a scalar weight. The d by d interaction block that corresponds to a single bond in the Hessian matrix can be written as $H_{ij\alpha\beta} = -V''|u_\parallel|^2 - \frac{V'}{r_{ij}}|u_\perp|^2$. The first term is often referred to as the stiffness while the second term is called the prestress term [31].

Interestingly, observations in 3D jammed packings suggest that the ω^4 regime only exists when the V' term is unperturbed; even very small perturbations to the prestress [3] open up a gap in the density of states [32]. This suggests that a self-organized balance between the stiffness and prestress must occur in systems near isostaticity. Moreover, the stiffness is always positive and the prestress always decreases the entries in the Hessian, so it is plausible that the prestress term is driving some interactions to be very weak near isostaticity. This is similar to our simple model where self-organized weak interactions also dominate the low-energy excitations. Therefore, it may be the case that the fine-tuning of α necessary in our model corresponds to fine-tuning in the prestress in real glasses. To investigate this possibility, future research will focus on studying the statistics of interparticle interactions to quantify the effective stiffness of bonds [33] in simulated glasses as the prestress is perturbed away from marginality [3].

In addition, a more concrete connection will require us to extend the insight from our simple model to higher dimensions. We see an ω^4 regime when bond strengths are uniform, but it is unclear what quantity would be analogous to a uniform bond weight in a $d \times d$ sub-block in a random matrix. Concurrent work by Benetti et al focused on d-dimensional Laplacian matrices where the magnitude of each bond is unity, but the geometry of the bond is randomly distributed, and these also generate scaling consistent with ω^4 at low frequencies [34]. Benetti et al. show this scaling in a higher-dimensional model also requires a network that is nearly isostatic. We are hopeful that in future work we may be able to connect our analytic results to these numerical ones in higher dimensions. One possible avenue is to study whether the geometric disorder in the model by Benetti et al. requires some interactions between nodes to be effectively zero along special soft directions.

Furthermore, although ω^4 scaling as been observed in several glass forming systems [7], the ω^3 regime may be unique to 1D systems, as it has not been reported in simulations or in the random matrices with 3×3 sub-blocks [34]. In addition, we see about half a decade of frequency consistent with ω^4 scaling, while the most recent data from Lerner and collaborators [7, 9, 32] finds almost a full decade.

Nevertheless, the ω^3 scaling regime is interesting. Disordered rings are well-studied, but major results focus on localization caused by disorder [35, 36]. To our knowledge, the finite-size scaling effects of the vibrational spectrum have not been discussed previously. Our model demonstrates that finite size effects in the disordered ring, such as this gapless low-frequency scaling, can be promoted into properties that are maintained in the thermodynamic limit by network disorder.

Although we have excellent understanding of the ω^3 regime in this simple model, and convincing numerical evidence demonstrating $D(\omega)$ is consistent with ω^4 scaling over a window of about half of a decade in ω, we have not identified a mechanism to understand this regime, where we know the assumption of two weak bonds and two rigid arms breaks down. In this analysis we have restricted ourselves to two-cuts, where only two weak bonds are involved in a mode. However, one can consider higher order cuts, where we remove more than two bonds, and yet which still have relatively low energies.These higher order cuts have been left for future work due to the specialized techniques for finding such partitions, like spectral clustering [37], which are beyond the scope of this work.

One possible avenue for understanding this regime is suggested by recent numerical work that shows universality in the eigenvector statistics associated with the boson peak. Specifically, eigenstatistics in jammed packings match those from both the random matrix model described here, as well as the dense limit of this model where all nodes are connected to one another [6]. Interestingly, the eigenvector statistics are also identical in a much simpler model which is just the sum of a diagonal matrix and a Gaussian orthogonal matrix. Very recent analytic work suggests that such matrices are marginal; they are on the edge of a non-ergodic localized phase [38]. It would therefore be very interesting to extend this analytic work to sparse matrices and study the tail of the density of states.

Another way to extend our model is to alter the loop structure of the underlying graph. In our random matrix

model, the loop structure is uncontrolled since we add crossbonds with uniform probability across the graph. This is different from jammed systems where neighbors of one particle are more likely to be neighbors of each other and loops are small. It is fairly straightforward to extend our analytic analysis of the ω^3 regime to random matrix models with smaller loops, and we expect that the prefactor and the onset of the scaling ω_e will change, but the ω^3 scaling will not. However, this change could impact the behavior of the ω^4 regime.

Acknowledgements We thank Fernanda Benetti, Gabriele Sicuro, and Giorgio Parisi for discussions. This work was partially supported by the Simons Foundation grant number 454947 (ES, PM, MLM), and by NSF-DMR-1352184 (ES, MLM). Computational resources were provided by support from Syracuse University and NSF ACI-1541396.

[1] M. L. Manning and A. J. Liu, Physical Review Letters **107** (2011).
[2] C. S. O'Hern, L. E. Silbert, A. J. Liu, and S. R. Nagel, Physical Review E **68** (2003).
[3] E. DeGiuli, A. Laversanne-Finot, G. Düring, E. Lerner, and M. Wyart, Soft Matter **10**, 5628 (2014).
[4] M. Wyart, S. R. Nagel, and T. A. Witten, Europhysics Letters (EPL) **72**, 486 (2005).
[5] L. E. Silbert, A. J. Liu, and S. R. Nagel, Physical Review Letters **95** (2005).
[6] M. L. Manning and A. J. Liu, EPL (Europhysics Letters) **109**, 36002 (2015).
[7] E. Lerner, G. Düring, and E. Bouchbinder, Physical Review Letters **117** (2016).
[8] H. Mizuno, H. Shiba, and A. Ikeda, Proceedings of the National Academy of Sciences **114**, E9767 (2017).
[9] G. Kapteijns, E. Bouchbinder, and E. Lerner, "Universal non-phononic density of states in 2d, 3d and 4d glasses," (2018), arXiv:1803.11383.
[10] P. Charbonneau, E. I. Corwin, G. Parisi, A. Poncet, and F. Zamponi, Physical Review Letters **117** (2016).
[11] G. Parisi and F. Zamponi, Reviews of Modern Physics **82**, 789 (2010).
[12] M. Baity-Jesi, V. Martín-Mayor, G. Parisi, and S. Perez-Gaviro, Physical Review Letters **115** (2015), 10.1103/physrevlett.115.267205.
[13] S. Wijtmans and M. L. Manning, Soft Matter **13**, 5649 (2017).
[14] A. Tanguy, B. Mantisi, and M. Tsamados, EPL (Europhysics Letters) **90**, 16004 (2010).
[15] M. Tsamados, A. Tanguy, F. Léonforte, and J. L. Barrat, The European Physical Journal E **26**, 283 (2008).
[16] D. J. Ashton and J. P. Garrahan, The European Physical Journal E **30** (2009), 10.1140/epje/i2009-10531-6.
[17] C. Brito and M. Wyart, Journal of Statistical Mechanics: Theory and Experiment **2007**, L08003 (2007).
[18] H. S. Camarda and P. D. Georgopulos, Physical Review Letters **50**, 492 (1983).
[19] M. Mehta, *Random Matrices*, Pure and Applied Mathematics (Elsevier Science, 2004).
[20] G. Parisi, The European Physical Journal E - Soft Matter **9**, 213 (2002).
[21] V. Gurarie and J. T. Chalker, Physical Review B **68** (2003).
[22] R. Merris, Linear Algebra and its Applications **197-198**, 143 (1994).
[23] T. Aspelmeier and A. Zippelius, Journal of Statistical Physics **144**, 759 (2011).
[24] L. Erdős, A. Knowles, H.-T. Yau, and J. Yin, The Annals of Probability **41**, 2279 (2013).
[25] L. Erdős, A. Knowles, H.-T. Yau, and J. Yin, Communications in Mathematical Physics **314**, 587 (2012).
[26] .
[27] P. Erdos and A. Renyi, Publicationes Mathematicae Debrecen **6**, 290297 (1959).
[28] G. M. Cicuta, J. Krausser, R. Milkus, and A. Zaccone, Physical Review E **97** (2018), 10.1103/physreve.97.032113.
[29] For $\delta z = 0.1$ and $N = 500$ and 1000, we calculate 2×10^6 matrices and for $N = 2000$ and 4000, we calculate 522240 and 261120 matrices. For all other values, we calculate 10^6 matrices.
[30] N. Xu, V. Vitelli, A. J. Liu, and S. R. Nagel, EPL (Europhysics Letters) **90**, 56001 (2010).
[31] W. G. Ellenbroek, *Response of Granular Media near the Jamming Transition* (Leiden Institute of Physics, Institute-Lorentz for Theoretical Physics, Faculty of Science, Leiden University, 2007).
[32] E. Lerner and E. Bouchbinder, Physical Review E **97** (2018).
[33] E. Lerner and E. Bouchbinder, The Journal of Chemical Physics **148**, 214502 (2018).
[34] F. P. C. Benetti, G. Parisi, F. Pietracaprina, and G. Sicuro, "Mean-field model for the density of states of jammed soft spheres," (2018), arXiv:1804.02705.
[35] F. J. Dyson, Physical Review **92**, 1331 (1953).
[36] P. Dean, Proceedings of the Physical Society **84**, 727 (1964).
[37] U. von Luxburg, Statistics and Computing **17**, 395 (2007).
[38] D. Facoetti, P. Vivo, and G. Biroli, EPL (Europhysics Letters) **115**, 47003 (2016).
[39] J. E. Gentle, *Computational Statistics (Statistics and Computing)* (Springer, 2009).

Appendix A: Extremal statistics in the two-regular graph

In this section, we calculate the scaling for a ring of N particles and a ring with crossbonds where particles are bonded to their nearest neighbors and the strengths of those bonds, $\{b_i\}$, are chosen independently with the distribution $f(b)$. (It is also assumed that the masses of the particles are identical.)

The mode associated with exciting only the 2 weakest bonds is a very low energy mode. The calculation here is done by taking the 2 weakest bonds as they are, but assuming all other bonds are rigid.

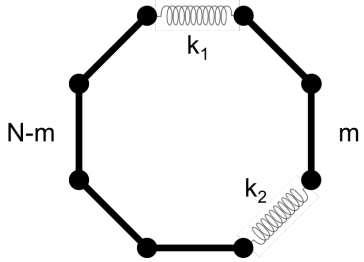

Figure 5: A ring or periodic 1d spring system with the two weakest bonds highlighted as springs.

We will call the strength of these bonds k_1 and k_2 with a distance of m nodes between the bonds. This system is equivalent to 2 masses joined by a spring which has 1 non-trivial mode with a frequency of $\sqrt{\frac{N(k_1+k_2)}{m(N-m)}} \equiv \sqrt{\frac{Ns}{m(N-m)}}$ where $s = k_1 + k_2$.

The distribution of the weakest bond strength is given by

$$\rho_1(k_1) = N * f(k_1) * (1 - F(k_1))^{N-1}, \tag{A1}$$

which is just the probability density of a bond having strength k_1 multiplied by the probability that all other bonds are at least that strong [39]. The distribution of the second lowest mode is somewhat more complicated since we need to enforce that $k_2 \geq k_1$. So the distribution of k_2 given k_1 is

$$\rho_2(k_2|k_1) = \frac{(N-1)\theta(k_2 - k_1)}{(1 - F(k_1))^{N-1}} f(k_2)(1 - F(k_2))^{N-2}. \tag{A2}$$

The frequency depends on the sum $s = k_1 + k_2$. The distribution of this sum can be obtained from the convolution of the distribution of k_1 and k_2.

$$\rho_s(s) = \int_{k_{min}}^{k_{max}} \rho_1(k_1)\rho_2(s - k_1, k_1)dk_1, \tag{A3}$$

$$\rho_s(s) = N(N-1)\int_{k_{min}}^{k_{max}} f(k_1)f(s-k_1) (1 - F(s-k_1))^{N-2}\theta(s - 2k_1)dk_1. \tag{A4}$$

By changing variables and assuming m is uniformly distributed, we can obtain the distribution of the frequencies as

$$\rho_\omega(\omega) = \sum_{m=1}^{N-1} \rho_s(\frac{m(N-m)}{N}\omega^2)\frac{2m(N-m)}{N(N-1)}\omega. \tag{A5}$$

1. Power Law Distribution

Let $f(b) = \frac{\alpha+1}{L^{\alpha+1}}b^\alpha$ and $F(b) = \left(\frac{b}{L}\right)^{\alpha+1}$ under the limit $b \in [0, L]$ and $\alpha > -1$. In the main text, we define $L = \frac{2+\alpha}{1+\alpha}$ such that the mean of the distribution is 1. By substitution, we find

$$\rho_s(s) = \frac{N(N-1)(\alpha+1)^2}{L^{2(\alpha+1)}}\int_0^L \theta(s-k_1)\theta(L-s+k_1) \theta(s-2k_1)k_1^\alpha(s-k_1)^\alpha\left(1 - \left(\frac{s-k_1}{L}\right)^{\alpha+1}\right)^{N-2} dk_1. \tag{A6}$$

These step functions are only non-zero in the range $max(0, s-L) \leq k_1 \leq s/2$. Using this information and a change of variables, $k = sq$, we can extract the primary contribution of s:

$$\rho_s(s) = s^{2\alpha+1}\frac{N(N-1)(\alpha+1)^2}{L^{2(\alpha+1)}}\theta(L - \frac{s}{2}) \int_{\max(0,1-\frac{L}{s})}^{\frac{1}{2}} q^\alpha(1-q)^\alpha\left(1 - \left(\frac{s(1-q)}{L}\right)^{\alpha+1}\right)^{N-2} dq. \tag{A7}$$

Under the assumption that s is small, such that $\left(1 - \left(\frac{s(1-q)}{L}\right)^{\alpha+1}\right)^{N-2} \approx 1$ (we will discuss the range of validity of this assumption below), the density of states for large N can be found via direct integration of $\int_0^{\frac{1}{2}}(q(1-q))^\alpha dq = \frac{\Gamma(\alpha+1)^2}{2\Gamma(2\alpha+2)}$:

$$\rho_s(s) \approx s^{2\alpha+1}\frac{N(N-1)(\alpha+1)^2}{L^{2(\alpha+1)}}\frac{\Gamma(\alpha+1)^2}{2\Gamma(2\alpha+2)}, \tag{A8}$$

$$\rho_\omega(\omega) \approx \frac{N\Gamma(\alpha+1)^2(\alpha+1)^2}{\Gamma(2\alpha+2)L^{2\alpha+2}}\omega^{4\alpha+3}\sum_{m=1}^{N-1}\left(\frac{m(N-m)}{N}\right)^{2\alpha+2}. \tag{A9}$$

By converting the sum over m into a similar integral over $\frac{m}{N}$ we have

$$\rho_\omega(\omega) \approx \frac{\sqrt{\pi}(\alpha+1)^2(2\alpha+2)\Gamma(\alpha+1)^2}{2^{4\alpha+5}\Gamma(2\alpha+\frac{7}{2})L^{2\alpha+2}}N^{2\alpha+4}\omega^{4\alpha+3}. \tag{A10}$$

Since this only applies to the lowest vibrational mode, the density of states is given by ρ_ω/N:

$$D(\omega) \approx \frac{\sqrt{\pi}(\alpha+1)^2(2\alpha+2)\Gamma(\alpha+1)^2}{2^{4\alpha+5}\Gamma(2\alpha+\frac{7}{2})L^{2\alpha+2}}N^{2\alpha+3}\omega^{4\alpha+3}. \tag{A11}$$

Appendix B: Extremal statistics in the two-regular graph with additional bonds

A more generic system is the ring with crossbonds. These crossbonds are simply additional connections between particles that are non-adjacent in the ring. See Figure 6 for an example of a crossbonded graph; although the sketch is 2 dimensional the cross bond interaction only depends on the distance along the ring not the euclidean distance across the ring.

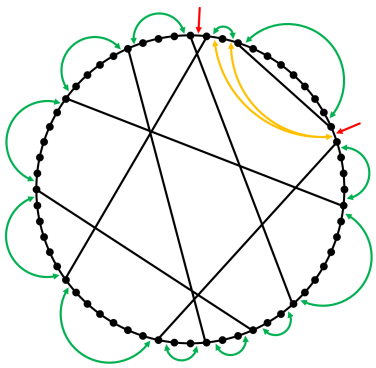

Figure 6: A sketch of a crossbonded network with 56 particles and 7 crossbonds. The green arrows delineate the regions between crossbonds where 2 edges can disconnect the network. The red arrows point out edges that can't disconnect the network. The yellow arrows point out sets of edges that would disconnect the network that aren't between crossbonded nodes.

With crossbonds, we are restricted to choosing bonds in a region between 2 crossbonded nodes. These regions are shown in Figure 6 by the green arrows.

1. Distribution of Bounded Regions

Let m_1 be the number of edges between crossbonded nodes.

We place the cross bonds randomly. Therefore the crossbonded nodes are chosen uniformly. If we have E crossbonds then there are $2E$ crossbonded nodes (which may not be unique). The increase in average coordination number is given by $\delta z = \frac{2E}{N}$. So the number of crossbonds and crossbonded nodes are $\frac{N\delta z}{2}$ and $N\delta z$ respectively.

Since these are uniformly placed, we can expect the distance between them to be defined via a Poisson process. We can find the distribution of the second crossbonded node where we set the first crossbonded node to 1, since we can always rotate along the ring. Order statistics provide the following result:

$$p_1(m_1) = \frac{(1-\frac{m_1}{N})^{N\delta z-1}}{\sum_{m=0}^{N-1}(1-\frac{m}{N})^{N\delta z-1}} \approx \frac{e^{\delta z}-1}{e^{\delta z}} e^{-m_1\delta z}. \quad \text{(B1)}$$

This distribution very quickly approaches the thermodynamic expression of an exponential decay.

2. Crossbonded Spectrum

For each chain of length m_1, we choose the 2 weakest bonds where the bonds are chosen from the distribution $f(b) = \frac{\alpha+1}{L^{\alpha+1}} b^\alpha$ under the limit $b \in [0, L]$ and $\alpha > -1$. In the main text, we define $L = \frac{2+\alpha}{1+\alpha}$ such that the mean of the distribution is 1. We can write $\rho_s(s)$ as

$$\rho_s^{m_1}(s) = \frac{(\alpha+1)^2 m_1(m_1-1)}{L^{2(\alpha+1)}} s^{2\alpha+1}\theta(L-\frac{s}{2}) \int_{max(0,1-\frac{L}{s})}^{\frac{1}{2}} q^\alpha(1-q)^\alpha \left(1-\left(\frac{s(1-q)}{L}\right)^{\alpha+1}\right)^{m_1-2} dq. \quad \text{(B2)}$$

We assume small s, such that $\left(1-\left(\frac{s(1-q)}{L}\right)^{\alpha+1}\right)^{m_1-2} \approx 1$. Following the same argument from the previous section where m_2 is the number of nodes between the weakest bonds, we find the distribution:

$$\rho_\omega(\omega) = \omega^{4\alpha+3}\frac{\Gamma(\alpha+1)^2(\alpha+1)^2}{2\Gamma(2\alpha+2)L^{2\alpha+2}}\frac{e^{\delta z}-1}{e^{\delta z}} \sum_{m_1=2}^{N-1} e^{-m_1\delta z} m_1 \sum_{m_2=1}^{m_1-1}\left(\frac{m_2(N-m_2)}{N}\right)^{2\alpha+2}. \quad \text{(B3)}$$

We take the thermodynamic limit and approximate the sums as integrals (over $x = \frac{m_i}{N}$ and $dx = \frac{1}{N}$) and expand the result in the low δz limit to obtain:

$$\rho_\omega(\omega) = \frac{\Gamma(2\alpha+5)\Gamma(\alpha+1)^2(\alpha+1)^2}{2(2\alpha+3)\Gamma(2\alpha+2)L^{2\alpha+2}}\frac{\omega^{4\alpha+3}}{\delta z^{2\alpha+4}}. \quad \text{(B4)}$$

Importantly, this is not just for the smallest mode. Since there are several regions on the ring from which pairs can be chosen, this analysis an extensive fraction of modes. On average, there are $N\delta z$ regions separated by crossbonded nodes. Therefore, we can apply this analysis for the lowest $N\delta z$ modes of a total N modes, ie. a fraction of modes δz. The density of states is given by $\rho_\omega(\omega) * \delta z$

$$D_\alpha(\omega) = \frac{\Gamma(2\alpha+5)\Gamma(\alpha+1)^2(\alpha+1)^2}{2(2\alpha+3)\Gamma(2\alpha+2)L^{2\alpha+2}}\frac{\omega^{4\alpha+3}}{\delta z^{2\alpha+3}}. \quad \text{(B5)}$$

Note that $\alpha = 0$, the uniform distribution, is unique in that ω and δz have the same exponent

$$D_0(\omega) = \frac{4}{L^2}\left(\frac{\omega}{\delta z}\right)^3. \quad \text{(B6)}$$

3. Full Spectrum

In the full spectrum we need to identify the frequency, ω^*, at which the spectrum crosses over into a plateau. In disordered solids, there are ample examples of this cutoff scaling linearly with δz; this is also true for the

disordered ring with crossbonds. ω_e only scales linearly with for $\alpha = 0$. Therefore it is only for $\alpha = 0$ that the scaling between ω_e and ω^*, ψ is independent of δz.

So the full spectrum of $\alpha = 0$ is given by:

$$D(\omega) = \begin{cases} \frac{4}{L^2}\left(\frac{\omega}{\delta z}\right)^3 & \omega \leq \omega_e \\ \left(\frac{4\omega_e^{3-\psi}}{L^2\delta z^3}\right)\omega^\psi & \omega_e \leq \omega \leq \omega^* \\ c & \omega^* \leq \omega \end{cases}. \tag{B7}$$

In practice, ψ is consistent with 4.

δz	ψ
0.1	4.0761
0.168	4.0115
0.282	3.9606
0.476	3.9496
0.8	3.9749

(B8)

4. Behavior of Sloshing Modes

The value of the IPR for a sloshing modes depends explicitly on the distance between the active bonds. If the active bonds are separated by m particles the IPR is given by

$$Y = \frac{1}{m} + \frac{1}{N-m} - \frac{3}{N}. \tag{B9}$$

Thus the increasing of the IPR plateau with δz in the sloshing regime is indicative of a decrease in the distance between active bonds. By construction of the crossbonded system, the distance between active bonds is limited by the distance between crossbonded nodes, which decreases with δz.

In low-frequency regime the IPR is independent of system size, while modes in the boson peak is strongly dependent on system size. We find that the low frequency regime is collapses; the behavior of the system below ω^* is independent of system size.

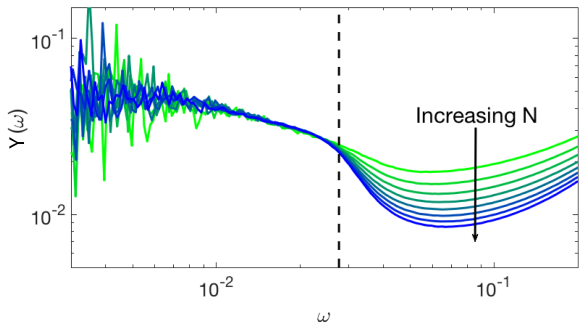

Figure 7: IPR at a fixed $\delta z = 0.1$, with system sizes varying from 300 to 1000 in steps of 100. The black dashed line indicates ω^*.

We can also measure the participation of the bonds with what we call the Bond Inverse Participation Ratio (BIPR):

$$Y_b(\omega) = \frac{\sum_{(i,j)}(v_i - v_j)^4}{(\sum_{(i,j)}(v_i - v_j)^2)^2}, \tag{B10}$$

where (i, j) is an edge in the network. In the limit of low frequency, there is a plateau of $BIPR = \frac{1}{2}$ which indicates that only 2 bonds are extending or compressing for the modes in that regime. This is secondary confirmation that the sloshing mode assumption is reasonable for this simple model.

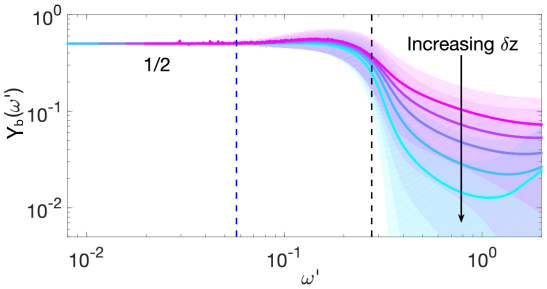

Figure 8: The BIPR with the frequency rescaled by δz, $\omega' = \omega/\delta z$. The blue dashed line indicates ω_e while the black dashed line indicates ω^*.